Memoirs of the Faculty of Engineering, Nagoya University
Vol. 33, No. 1 (1981) — Research Report —

MEASUREMENTS OF LOW DENSITY, HIGH VELOCITY FLOW BY ELECTRON BEAM FLUORESCENCE TECHNIQUE

TAKEO SOGA, MASAYA TAKANISHI and MICHIRU YASUHARA

Department of Aeronautical Engineering

(Received July 1, 1981)

Abstract

A low density chamber with an electron gun system was made for the measurements of low density, high velocity (high Mach number) flow. This apparatus is a continuous running facility. The number density and the rotational temperature in the underexpanding free jet of nitrogen were measured along the axis of the jet by the electron beam fluorescence technique. The measurements were carried out from the vicinity of the exit of the jet to far downstream of the first Mach disk. Rotational nonequilibrium phenomena were observed in the hypersonic flow field as well as in the shock wave (Mach disk).

I. Introduction

The unconfined free jet expansion from a sonic orifice into a vacuum (Fig. 1) has been used as a source of high velocity (high Mach number), low density gas flow.[1~7] Chemical phenomena in the rocket exhaust at an upper altitude atmo-

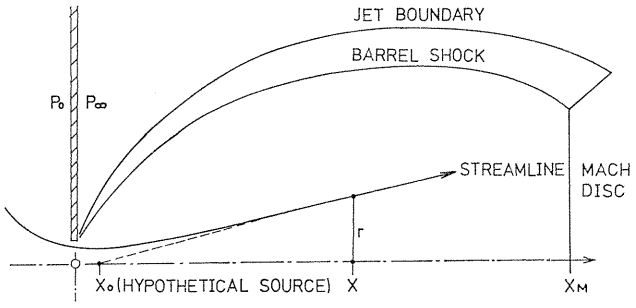

Fig. 1. Sketch of free jet flow field.

shere[8,9] as well as their aerodynamics[10,11] were also studied using such free jet expansions. Experiments of isotope separations by means of the laser optics[12] as well as by the aerodynamical methods[13] were intensively carried out by many investigators where a molecular beam or a free jet expansion was used.

For last two decades, on the other hand, the electron beam fluorescence technique was well developed for the measurements of flow properties in the low density free jets; by this technique, a number density of gases or a rotational temperature of diatomic gases in any small portion of the flow is measurable[14,15] without disturbing the flow to any significant extent. The rotational temperatures in the free jets and shock waves were measured by Robben et al.[16] and Marrone.[17] Muntz[18] measured the velocity distribution function of flowing gas with the aid of the Fabry-Perot etalon interferometer, from which the translational temperature and the flow velocity are obtained. Many other experiments concerned with the electron beam fluorescence technique are summarized in AGARD 132 by Muntz.[19] Recent studies can be found in the proceedings of the International Symposium of Rarefied Gas Dynamics.[20]

In spite of the large volume of the accumulation of the free jet experiments, various types of aerodynamics and chemical physics in the jet are still remained to be studied; for example, jet interactions, isotope separations, condensation phenomena and so on. In this report, our preliminary studies on the free jet experiments are presented; as the first step, the density and the rotational temperature along the centerline of the free jets were measured from the vicinity of the orifice to far downstream of the first Mach disk.

Ⅱ. Electron Beam Fluorescence Technique

The emission or fluorescence excited by an energetic electron beam will have a spectrum peculiar to the composition and temperature of the gas through which the beam passes. A detailed analysis of the beam-excited emission in the nitrogen gas has been presented by Muntz[19] and is only outlined here.

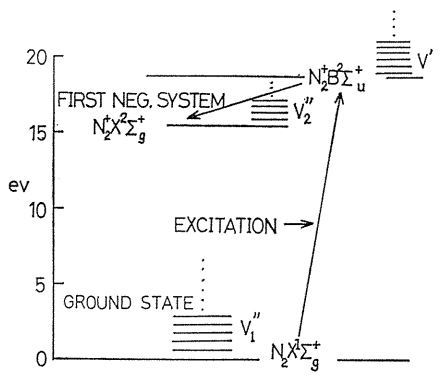

Fig. 2. Excitation and emission paths for the first negative system of nitrogen.

The excitation emission path is indicated shematically in Fig. 2. The energetic electrons excite and ionize the ground state nitrogen molecules ($N_2X^1\Sigma$) up to the excited state of the molecular ion ($N_2^+B^2\Sigma$), then, complises the first negative system. The intensity I_{jk} of the band spectrum corresponding to $j \rightarrow k$ transition, is propotional to the local species concentration, n_g, at low pressure:

$$I_{jk}=ch\nu_{jk}A_{jk}n_g \; : \; A_{jk}=n_e v_e Q_{oj},$$

where jk implies the transition from the j state to the k state, and h denotes Plank's constant, c the speed of light, ν_{jk} the wave number of the emission, A_{jk}

Einstein's transition probability, n_e the number density of the electron beam, v_e the speed and $Q_{oj}(v_e)$ the cross section of the transition from the ground state to the j state. For a given electron beam condition and the transition ($j \rightarrow k$), I_{jk} becomes a measure of n_g.

In the extensive form, I_{jk} is given as

$$I_{jk}=Kn_g/\left(1+\frac{2n_gQ_{gg}v_{gg}}{A_{jk}+A_T}\right) : K=hc\nu_{jk}n_ev_eQ_{oj}.$$

Here, A_T is the sum of A_{mn} (m, $n \neq j$, k), Q_{gg} is the cross section for the quenching collisions and $\bar{v}_{gg}$ is the thermal velocity of gas molecule. As n_g increases, the second term in the denominater becomes significant. Eventually, the emission saturates at the value,

$$I_{jk}=K(A_{jk}+A_T)/(2Q_{gg}v_{gg})=Kn_g^*.$$

The linearity of I_{jk} against n_g is, then, valid for $n_g \ll n_g^*$; for the 0–0 band of the first negative system of nitrogen, n_g^* is the number density corresponding to the pressure of about 0.5 Torr at room temperature.

For a gas in thermal equilibrium, the population N_K of the K rotational level in the v'' vibrational level is proportional to (Herzberg)[22]

$$N_K \propto (2K+1)\exp[-K(K+1)(B_{v''}hc)/kT_R]$$

where $B_{v''}$ denotes the molecular rotational constant of the vibrational level v'', and k Boltzmann's constant. Here, the quantum number J is replaced by K, a quantum number of the rotation of nucli (See Ref. 14). At room temperature or less, there is no vibrational excitation of importance in the case of nitrogen, *i. e.*, $v''=0$. The combination $B_0hc/k=\theta_R$ is the characteristic rotational temperature of the molecule; for the nitrogen molecule, $\theta_R=2.8779°K$.

In emission from K' in $(N_2^+B^2\Sigma)_{v'=0}$ to K'' in $(N_2^+X^2\Sigma)_{v''=0}$, the intensity depends on the mean value of $(2K+1)$ for the upper and lower states (Herzberg[22]). If the assumption is made that the ground state nitrogeo molecnles before excitation by the electron beam has a Boltzmann distribution of rotational energy at a rotational temperature, T_R, and that the excitation from $N_2X^1\Sigma$ to $N_2^+B^2\Sigma$ is governed by the optically allowed selection rules (dipole transition), it is possible to predict the line intensity of 0–0 vibrational-rotational band. Muntz's relation is given as

$$(I_{K'K''})_{v'v''}=(K'+K''+1)C[G](\nu/\nu_0)^4\exp[-K'(K'+1)(\theta_R/T_R)]$$

where C is a constant. The factor $[G]$, which includes the Honl-London rotational transition probability, is given as

$$[G]=\frac{(K'+1)\exp[-2(K'+1)(\theta_R/T_R)]+K'\exp[2K'(\theta_R/T_R)]}{2K'+1}.$$

In the optically allowed transition, $\Delta K=\pm 1$, which results in the formation of P-branch (whose lines are spaced toward the red until this branch doubles back on itself forming a band head) and R-branch (whose lines are spaced toward violet end of the spectrum) in the rotational fine structure. For the 0–0 band in the first negative system, the band origin ($K'=0$) is at 3909A° and the band head due

to P-branch folding back lies at 3914A°.

The log slope technique can be used for the R-branch to obtain the value of T_R:

$$\log\frac{(I_{K'K''})_{v'v''}}{(K'+K''+1)[G](\nu/\nu_0)^4}=-\frac{\theta_R}{T_R}K'(K'+1)+\text{const}\,. \qquad (1)$$

Plotting the left side versus $K'(K'+1)$ will yield a straight line with a slope, $-\theta_R/T_R$, from which T_R is obtained. Since $[G]$ includes T_R, the procedure is iterative.

Coe et al.[21] proposed a multi-interaction dipole-quadrapole transition model where $[G]$ is given as

$$[G(K')]=(1/B_{K'}(T_R))\sum_{K=1}^{\infty}{}_KE_{K'}(p_i)B_K(T_R)\ :$$

$$B_K(T_R)=(2K+1)\exp[-K'(K'+1)\theta_R/T_R]$$

where ${}_KE_{K'}(p_i)$is an element of matrix E which expresses all possible multi-interactions of the transition from K to K'. A probability, p_i (which is included in ${}_KE_{K'}$) that the over all interactions will consist of "i" quadrapole interactions in addition to the initial dipole interaction, is evaluated experimentally by finding the values p_i which give the best straight line fit to the spectroscopic data sample. For the measurements of very low temperature, *i. e.*, T_R of several times of θ_R, such "elaborated" transition model may be necessary.

Ⅲ. Experimental Apparatus

The experimental apparatus used in this experiment consists of (1) low density chamber with vacuum systems, (2) an electron gun system for generating the electron beam, (3) plenum chamber with a sonic orifice; the plerum chamber is mounted on a traverse unit, and (4) optical systems measuring the luminosity of the light emitted from the concerned segment of the electron beam.

(1) The low density chamber.

In Fig. 3 is shown a shematic diagram of the low density chamber(LC) with the electron gun in place. External views of LC are given in Fig. 4. The LC, which has a dimension 100cm in diameter and 160cm in length, is a continuous running facility having two primary pumping systems. The one is the 14″ oil vapor diffusion pump(DP) for high vacuum experiments, which has a pumping capacity of approximately 5500 liters/sec. (5KW at 200V. AC.) at chamber test section pressure lower than 0.1m Torr and is connected to the second stage of pumping of the oil rotary pump(RP1) which has a 3000 liters/min. capacity (5 HP at 200V. AC.). The other one is the 14″ oil vapor diffusion-ejector pump(DEP) which has the maximum pumping speed, 4000 liters/sec. at about 1mTorr, and its back pressure is evacuated by a 5 HP oil rotary pump(RP2) having a 3900 liters/min. pumping capacity. The switch of the power supply to the vacuum systems is connected with a relay, by which the electricity is turned off when the cooling water supply is stopped. Main valves of DP and DEP, which connect the pumps with the test chamber, auxiliary

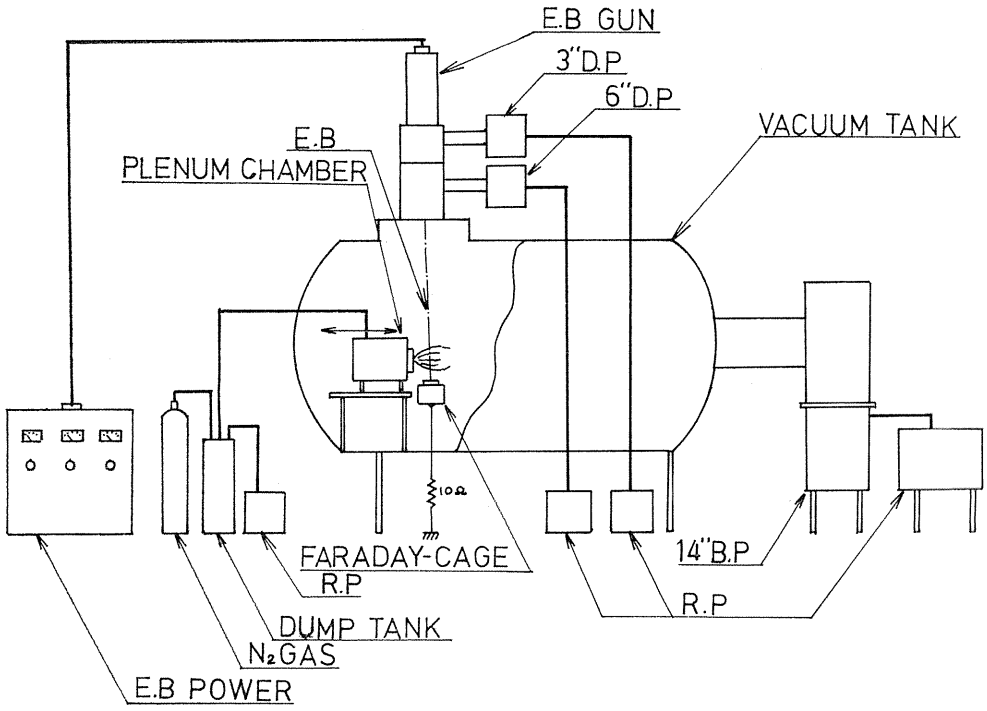

Fig. 3. Schematic diagram of the low density chamber with electron gun.

valves which connect DP and DEP with RP1 and RP2, respectively, and leak valves of RP1 and RP2 are operated using high pressure air (about 4 atm.) compressed and reserved in a 1 HP mini-compressor. At the instance electricity to the pumps is turned off accidentally, all valves are shut down so as to isolate each pump systems and the rotary pumps are automatically vented.

The pressure in the test chamber can be made lower than 0.02m Torr by use of DP system without issuing the gases from the orifice at the plenum chamber. When the gas is issued, the pressure of the chamber becomes higher than the ultimate pressure without gas flow and DEP pump system becomes preferable to the experiment. The maximum pumping speed gives the maximum size of the flow field shown in Fig. 1. The distance from the sonic orifice to the first Mach disk, X_M is simply proportional to the square root of the volumetric pumping speed, $\overline{V}^{1/2}$, independent of the orifice diameter (Ashkenas anp Sherman[2]);

$$X_M(\mathrm{cm}) = (4/3\sqrt{\pi})(\gamma RT_0)^{-1/4}\{(\gamma+1)/2\}^{(\gamma+1)/4(\gamma-1)}\overline{V}^{1/2}(\mathrm{cm}^3/\mathrm{s.})$$

where γ is the specific heats ratio.

In other expression,

$$X_M/D = (2/3)(p_0/p_\infty)^{1/2},$$

where p_0 is the pressure in the plenum chamber and p_∞ is that in the test chamber. Under the maximum pumping speed (4000 liters/sec. at p_∞=1m Torr), the maximum

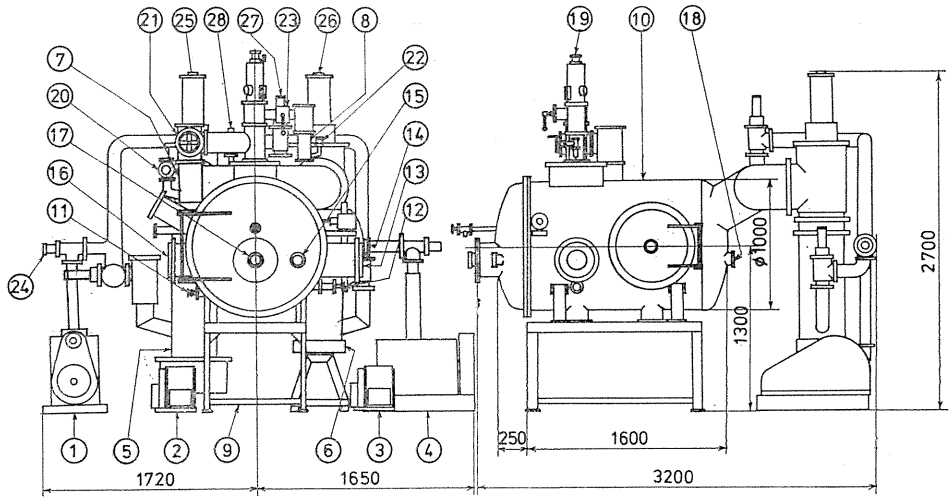

1. Oil rotary pump (RP)
2. RP3 (1 HP)
3. RP4 (1 HP)
4. RP1 (5 HP)
5. Oil vapor diffusion-ejector pump (DEP) (14″, 15 KW)
6. Oil vapor diffusion pump (DP) 1 (14″, 5 KW)
7. DP2 (6″, 1 KW)
8. DP3 (3″, 0.5 KW)
9. Stand of the chambər
10. Low density chamber
11. Handle of the traverse unit
12. ibid
13. Optical window (ϕ150)
14. Observing window (ϕ97)
15. ibid
16. Optical window (ϕ150)
17. Observing window (ϕ97)
18. ibid
19. Electron gun
20. Auxiliary valve of DEP
21. Main valve of DP2
22. Auxiliary valve of DP1
23. Main valve of DP3
24. Leak valve of RP2
25. Main valve of DEP
26. Main valve of DP1
27. Valve for preliminary evacuation of the chamber
28. Leak valve of the chamber

Fig. 4. External view of the experimental apararus.

distance is about 10.5cm. For the normally operating condition ($p_\infty \approx$30m Torr), $X_M=4.5$cm.

If the pressure, p_∞ is kept constant, then, the mass flux (which is proportional to p_0D^2) is fixed. For $p_0D^2=105$ Torr-mm^2, which gives $X_M=4.5$cm for $p_\infty=30$m Torr, jet Reynolds number is given by

$$R_{eD}=2030/D\,(\mathrm{mm})$$

(2) The electron gun

The electron gun assembly for weldering (EBW, S/N 522 type) is mounted atop the chamber test section (Fig. 5). The electron beam produced by the electron gun passes through both the aperture bored on the bottoms of the gun chamber and the intermediate pressure chamber, which separates the gun chamber from the test section of LC. In the present experiment, the upper aperture is removed. The lower aperture has a diameter of 3mm with 4 mm in length. A 3″

DP (capacity of 360 liters/sec.) maintains the gun chamber pressure 0.02 ~0.2m Torr under normal operating conditions; test section pressure may be typically in the range, 1 ~ 200m Torr. The intermediate chamber is evacuated by the 6″ DP (capacity of 1200 liters/sec.) and its pressure is maintained less than 0.5m Torr.

The electron beam (EB) passing through the test gas is collected by a Faraday cage and the beam current is obtained by measuring the voltage drop across a 10ohm resistance inserted between the Faraday cage and the earth.

The alignment of EB is acheived by a set of electromagnetic deflection coils which are mounted below the electron gun. Then, EB is focused by an electromagnetic lens on the centerline of the free jet, which is done by setting a removable plate at the height of the centerline; the diameter of the focused EB on this plate is about 1.6 mm. The cathode potential can be varied from 0 to −45KV and the beam current can be varied in the range from 2 mA to 35 mA. In the present experiment, the beam current and the cathode potential were held at −15KV and 2 mA measured at the Faraday cage, respectively, and the anode is kept at the ground potential.

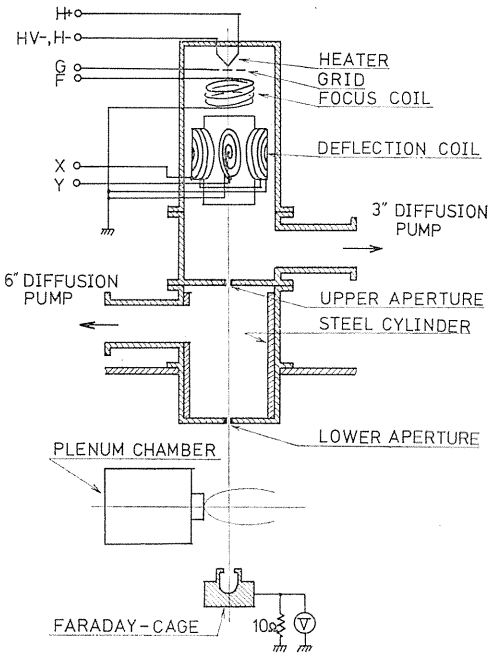

Fig. 5. Schematic diagram of the electron gun system.

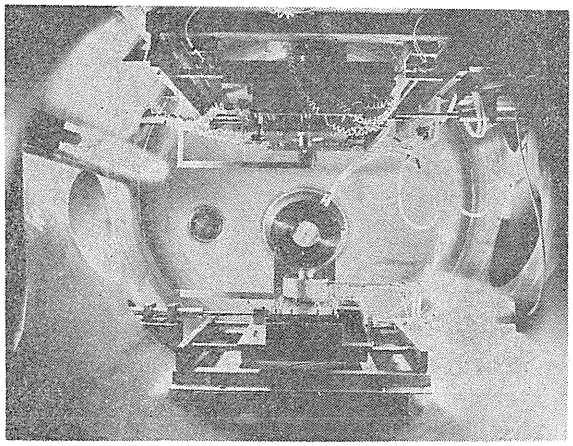

Fig. 6. Plenum chamber mounted on the movable unit.

(3) Plenum chamber and sonic orifice.

The plenum chamber (10cm in diameter and 13cm in length) is mounted on the movable table with which it is capable of traversing in a square of 18 cm a side (Fig. 6). Thin brass foil (0.05mm in thickness), on which 1 to 5 mm diameter hole is bored, is attached to a straight nozzle of 50 mm in diameter and 30 mm in length and this nozzle is fixed on one side of the plenum chamber. Test gases are issued from this sonic orifice into the test section, while the gases are

supplied through a teflon tube (10 mm in diam.) from a reservoir outside of LC.

(4) Optical systems.

As shown in Fig. 7, two optical systems are used. For the measurement of gas density, fluorescence from the EB is gathered with a lens and is focused on the slit in front of the photomultiplier (PM). Between the lens and the slit, the interference filter (Vacuum Opt. Co., Japan), which has a half width of 18Å around 3900Å, is laid and the light is made to pass through this filter. The light signal is measured using a HTV R105UH type PM, which has a S-4 spectral response (a peak at 4000Å). The output of PM versus the measuring position is directly recorded by the X-Y recorder.

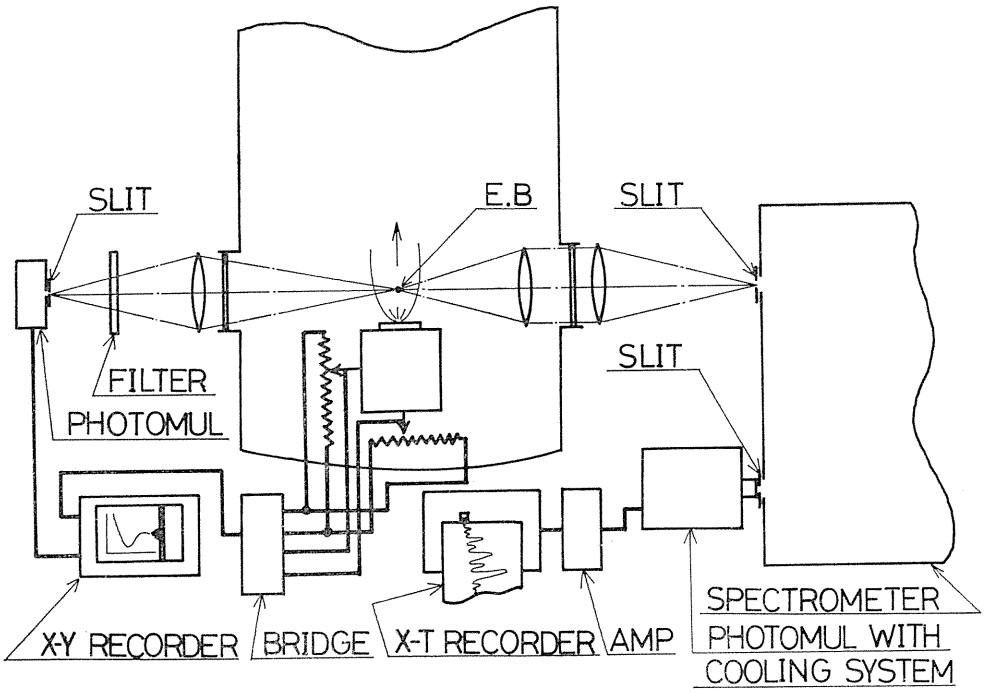

Fig. 7. Top view schematic of the optical systes.

In the spectroscopic system, the light from EB is collected and made parallel by the first lens in the chamber, which is further focused on the entrance slit of the spectrometer by the second lens in front of the slit. Jarell-Ash 78-490 type spectrometer is used to obtain the rotational spectrums. The spectrometer has a 102 mm square grating with 1180 rulings/mm and the focal length of 750 mm. The optical f number of the instrument is 6.5. The second order spectrums, with the dispersion of 4.7Å/mm are used. Rotation of the grating causes the resolved spectrums to move past the exit slit and the intensity of the lines is measured by a PM placed behind the exit slit. In the present experiment, the entrance slit width is 0.05 mm and the height is 0.5 mm. The exit slit width is the same as the

entrance slit width.

The PM used to measure the line intensity is cooled HTV R106UH type, having S-19 spectral response (a peak at 3400Å). The dark current measured as the noise of the output current is less than 0.2 nA at 750V when the PM is cooled to −15℃. The output of PM is amplified and recorded by the X-T recorder against the wave length.

Ⅳ. Experimental Results and Discussion

4. 1 Density measurement

In this experiment, the slit has a width of 1 mm and a hight of 0.2 mm. The magnification of this optical system is close to 1/2. Thus, the slit image on the EB is 2 mm in width, which makes it possible to eliminate the effects of the small fluctuation of EB.

The PM anode current, I_{ph}, was calibrated against a static nitrogen density at room temperature (24℃). The obtained curve (Fig.8) showa a slight nonlinearity as the pressure increases. This may be caused from the spreading of beam electrons; a decrease of the electron density in EB may reduce the fluorescence at the measuring point.

Nitrogen free jet was issued from a sonic orice of 5 mm in diameter and 0.05 mm in thickness; $t/D=0.01$. The experimental data presented in Ref. 2($t/D=0.027$) indicate that the effective orifice discharge coefficient is almost unity for $R_{eD}>100$. In the present experiment, p_0, p_∞ and p_0/p_∞ are 2.7 Torr, 22.5m Torr and 120, respectively. Resulting X_M and R_{eD} are 7.3 and 251, respectively. Thus, the D value used in the x/D correlation is the actual exit diameter of the orifice.

The measured density distribution along the jet centerline is shown in Fig. 9, where the output of PM were calibrated by the curve in Fig. 8. The results show an upward deviation from the isentropic distribution near the orifice, which may be atributed to the insufficient spatial resolution. The thickened (or diffused) Mach disk shown in Fig. 9 is characteristic in the transient regime of the free jet

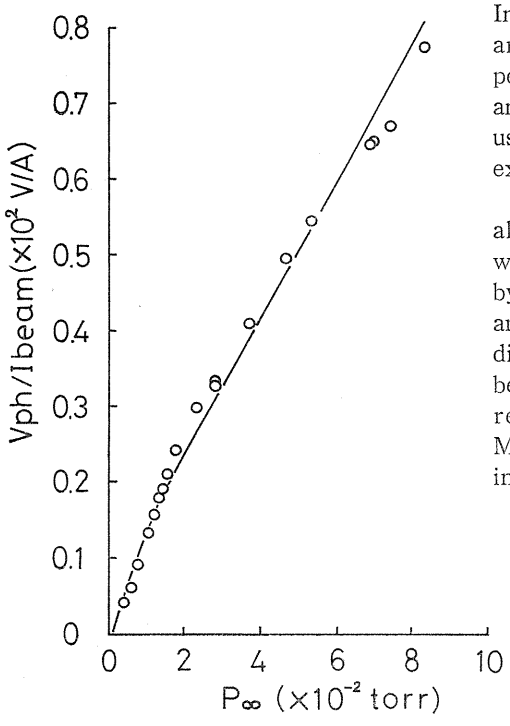

Fig. 8. Calibration curve of photo-multiplier current against gas pressure at room temperature (24℃).

experiment.[23] The overshoot of the density at the Mach disk is about 25% of the density of ambient gas, ρ_∞. When the location of the Mach disk is defined by $\rho(X_M/D) = \rho_\infty$, X_M obtained from Fig. 9 agrees well with the one predicted by Eq. (2).

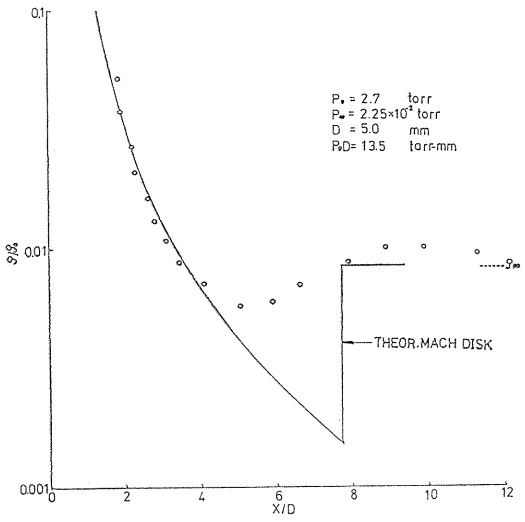

Fig. 9. Depsity distribution versus the axial distance, x/D.

4. 2. Rotational temperature measurement

Firstly, the rotational temperature of the ambient static gas was measured after removing the orifice (downstreamwards and was off centered) far away from EB, while the gas was issuing from the orifice. In this measurement, the height of the entrance slit of the spectrometer was set to 15 mm (in this case, the spatial resolution was unnecessary). The pressure of the ambient gas was 37. 5m Torr and the room temperature was 298°K. The beam was monitored during this interval and recorded by the X–T recorder. The fluctuation of the beam current was less than 5%.

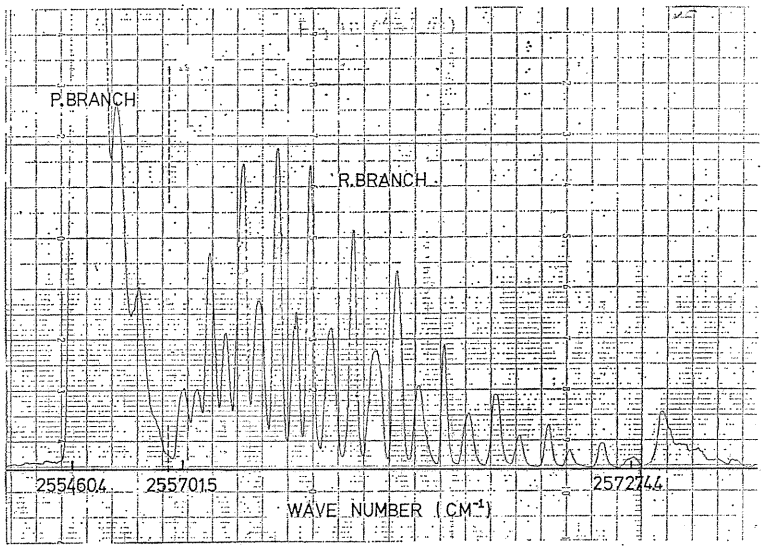

Fig. 10. Room temperature R-branch rotational spectrum of N_2^+ 0-0 band.

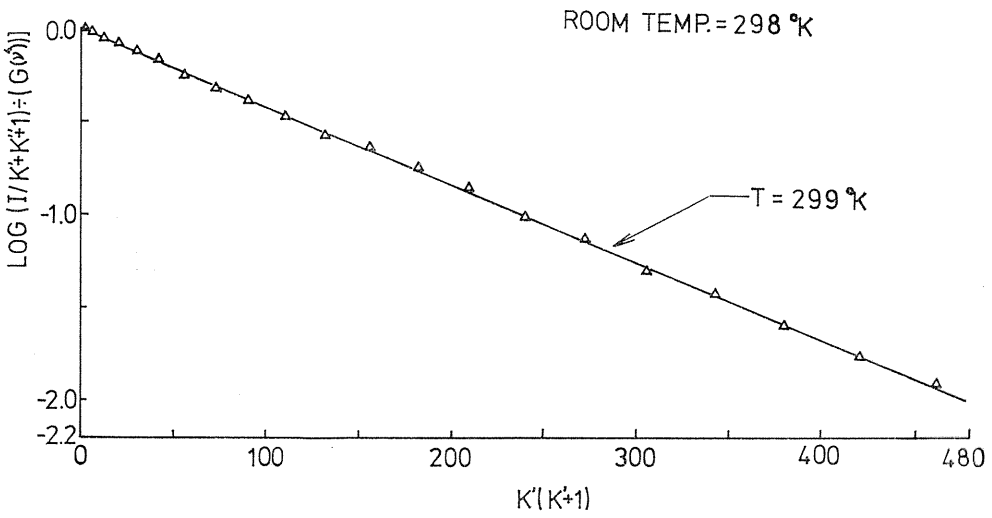

Fig. 11. Log slope plot of intensity of room temperature data.

A typical spectrums of the rotational fine structure in 0-0 band is shown in Fig. 10 where the speed of the rotation of the grating was such that the entire R-branch spectrums was obtained in approximately 2 minutes. Twenty-one rotational lines in the R-branch are seen, with the spacing between lines incresing with increasing K'. Owing to the nuclear spin properties of the nitrogen molecule, the alternate line intensities are predicted to be in the ratio of 2 : 1 on the $K'(K'+1)$ log plots at the same value of the ordinate. These half-intensity lines correspond to even values of K' as shown in the figure. For all data reduction, the heights of these lines were multiplied by two for use in the slope technique shown in Fig. 11. The rotational temperature obtained from this slope indicates 299°K, while the room temperature was 298°K. Agreement is remarkable. The rotational temperature distribution along the centerline of the free jet expansions from a 3 mm in diameter orifice was measured. Measurements were carried out from the orifice exit to far downstream of the first Mach disk. Important flow parameters of the nitrogen free jet are given in Table I.

Table 1. Nitrogen free jet flow conditions.

p_0D (Torr-mm)	D (mm)	p_0 (Torr)	p_∞ (m Torr)	p_0/p_∞	R_{eD}	X_M/D
20.4	3	6.8	35	194	677	9.3
21.0	3	7.0	37.5	187		9.2

For each data point along the jet centerline at a given p_0D value, the spectral data were analyzed as discussed in Sec. II and the rotational temperature, T_R, was obtained. A number of log slope plots are presented in Figs. 12 and 13 for the representative data points. The slopes of the linear portion were used to obtain

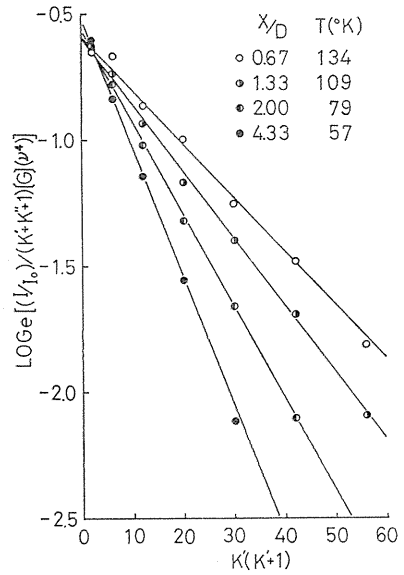

Fig. 12. Log slope plots of intensity of free-jet spectral data.

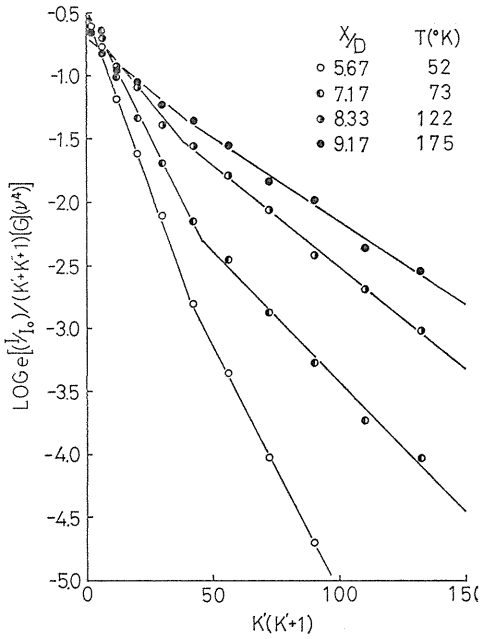

Fig. 13. Log slope plots of intensity of shock wave spectral data.

T_R. Higher K' lines are seen to depart from this linear curve (to upwards). In the shock wave, log plots curves have different two linear portions, which is substantial to the phenomena (See Fig. 13). The first slope for small K' is concerned with the rotational temperature ahead of the shock wave and it approaches gradually to the other slope The second slope is more gentle than the first one and, eventually, it approaches to the slope corresponding to the rotational temperature behind the shock wave. Since the rotational energy in the shock wave is far from the Boltzmann distribution, the rotational temperature can not be obtained from the log-plot technique and it should rather be obtained as the mean rotational energy. However, in this report, we estimate the rotational temperature from the first slope, only for convenience, which will give a steeper shock profile than the actual one.

The rotational temperature versus the axial distance, x/D, is plotted in Fig. 14. The errors of positioning are estimated to be about ± 1 mm due to the spatial fluctuation of the electron beam and those of temperature by the current fluctuation are estimated to be less than 5%.

At small values of x/D, the measured values of T_R fall on the isentropic curve for $\gamma=1.4$. The results show that the decrease of T_R along the isentropic curve is followed by a sudden increase of it due to the shock wave formation at the Mach disk. The temperature decrease behind the Mach disk shows a re-acceleration of the flow. Similar trend were observed in the previous measurement by one of the authors (M. Y.).[24]

Poulsen et al.[25] measured the terminal rotational temperature, of the free jet into extremely low pressure, by the time-of-flight method combined with the

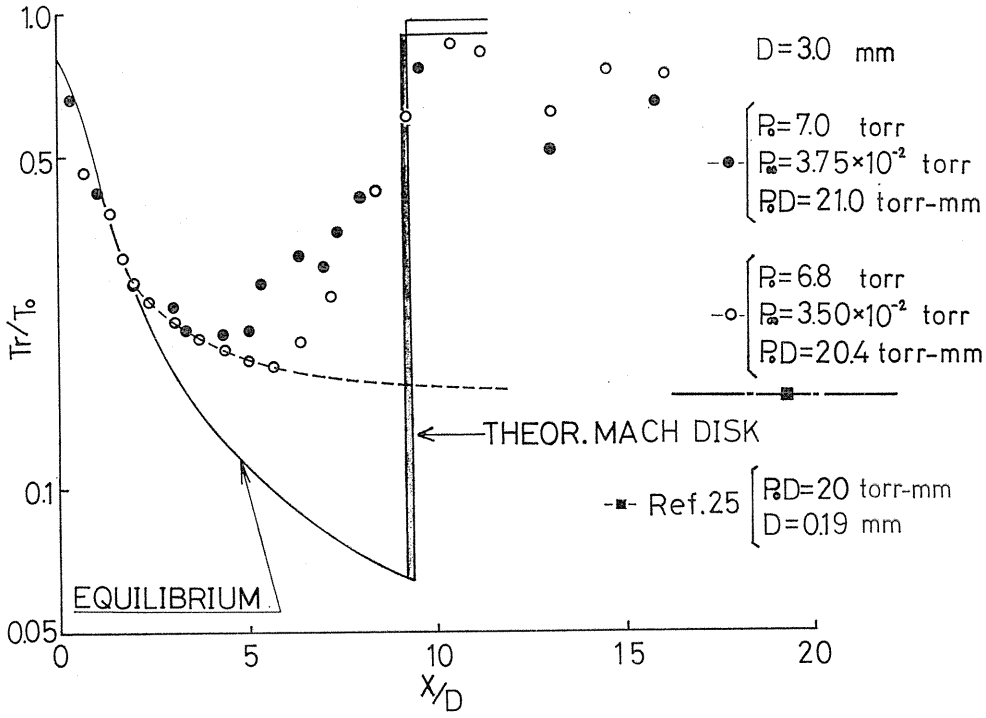

Fig. 14. Rotational temperature distribution along the axis of free jet.

electron beam fluorescence technique. Their result at $p_0D=20$ is also shown in Fig. 14. If there is no shock wave, the rotational temperature seems to approache to this terminal value.

The present work was partly supported by the scientific funds of the Ministry of Education, and the experimental data were analyzed using the FACOM 230-75 computer at the Computer Center, Nagoya University.

References

1) J. B. French, "Continuum-Source Molecular Beams", AIAA J, Vol. 3, No. 6, p. 993-1000 (1965).
2) H. Ashkenas and F. S. Shermann, "The Structure and Utilization of Supersonic Free Jets in Low Density Wind Tunnels", in Rarefied Gas Dynamics, edited by J. H. de Leeuw (Academic Press Inc., New York, 1966), Vol. Ⅱ, p. 84-105.
3) J. B. Anderson and J. B. Fenn, "Velocity Distributions in Molecular Beams from Nozzle Sources", Phys. Fluids, Vol. 8, No. 3, p. 780-787 (1965).
4) U. Bossel, F. C. Hurlbut and F. S. Sherman, "Extraction of Molecular Beams from Nearly-Invicid Hypersonic Free Jets", in Rarefied Gas Dynamics, edited by L. Trilling and H. Y. Wachman (Academic Press Inc., New York, 1969), Vol. Ⅱ, p. 945-964.
5) J. J. Smolderen, J. F. Wendt, J. Naveau and T. T. Bramlette, "Sphere and Cone Drag Coefficients in Hypersonic Transitional Flow", in Rerefied Gas Dynamics, edited by

L. Trilling and H. Y. Wachmann (Academic Press Inc., New York, 1969), Vol. I, p. 903-907.
6) K. Bütefisch, "Investigation of Hypersonic Non-Equilibrium Rarefied Gas Flow Around a Circular Cylinder by the Electron Beam Technique", in Rarefied Gas Dynamics, edited by L. Trilling and H. Y. Wachman (Academic Press Inc., New York, 1969), Vol. II, p. 1739-1748.
7) F. Robben and L. Talbot, "Measurement of Shock wave Thickness by the Electron Beam Fluorescence Method", Phys. Fluids, Vol. 9, No. 4, p. 633-643 (1966).
8) J. Leng, R. A. Oman and H. B. Hopkins, "A Detonation Tube Technique for Simulating Rocket Plumes in a Space Enviroment", J. Spacecraft and Rocket, Vol. 5, No. 10, p. 1148-1154 (1968).
9) T. Dwayne McCay and H. M. Powell, "Direct Mass Spectrometric Measurements in a Highly Expanded Rocket Exhaust Plume", J. Spacecraft and Rocket, Vol. 15, No. 3, p. 133-138 (1978).
10) R. D. Herron, "Jet-Boundary Simulation Parameters for Underexpanded Jet in a Quiescent Atomosphere", J. Spacecraft and Rocket, Vol. 5, No. 10, p. 1155-1160 (1968).
11) V. S. Calia and J. W. Brook, "Measurements of a Simulated Rocket Exhaust Plume Near the Prandtl-Meyer Limiting Angle", J. Spacecraft and Rocket, Vol. 12, No. 4, p. 205-208 (1975).
12) E. P. Muntz and B. B. Hamel, "Rarefaction Phenomena in Gas and Isotope Separations", in Rarefied Gas Dynamics, edited by M. Becker and M. Fiebig (DFVLR-Press, Porz-Wahn, West Germany, 1974), Vol. I, p. B. 1-1-B. 1-7.
13) E. P. Muntz and T. L. Deglow, "Rarefaction Phenomena in Gas and Isotope Separation with Emphasis on Jets and Beams", in Rarefied Gas Dynamics, edited by R. Campargue (COMMISSARIAT A L'ENERGIE ATOMIQUE, Paris, 1979) Vol. I, p. 573-586.
14) E. P. Muntz, "Static Temperature Measurements in a Flowing Gas", Phys. Fluids, Vol. 5, No. 1, p. 80-90 (1962).
15) E. P. Muntz and D. J. Marsden, "Electron Excitation Applied to the Experimental Investigation of Rarefied Gas Flows", in Rarefied Gas Dynamics, edited by J. A. Laurmann (Academic Press Inc., New York, 1963), Vol. II, p. 495-529.
16) F. Robben and L. Talbot, "Measurements of Rotational Temperatures in a Low Density Wind Tunnel", Phys. Fluids, Vol. 9, No. 4, p. 644-652 (1966).
17) P. V. Marrone, "Temperature and Density Measurements in Free Jets and Shock Waves", Phys. Fluids, Vol. 10, No. 3, p. 521-538 (1967).
18) E. P. Muntz, "Molecular Velocity Distribution-Function Measurements in a Flowing Gas", Phys. Fluids, Vol. II, No. 1, p. 64-76 (1968).
19) E. P. Muntz, "Electron Beam Fluorescence Technique", AGARD graph 132 (1968).
20) See reference 12 and 13 and also "Rarefied Gas Dynamics", edited by J. L. Potter (Progress in Astronautics and Aeronautics, Vol. 51, 1977).
21) D. Coe, F. Robben, L. Talbot and R. Cattolica, "Rotational Temperatures in Nonequilibrium Free Jet Expansion of Ntrogen", Phys. Fluids, Vol. 23, No. 4, p. 706-714 (1980).
22) G. Herzberg, "Molecular Spectra and Molecular Structure" (D. Van Nostrand Company, Inc., Princeton, 1950).
23) E. P. Muntz, B. B. Hamel and B. L. Maguire, "Some Characterictics of Exhaust Plume Rarefaction", Phys. Fluids, Vol. 8, No. 9, p. 1651-1658 (1970).
24) M. Yasuhara, "Rotational Temperature Measurement of the Flow Expanding from a Low Density Sonic Orifice", USCAE Rep. 103, Univ. Southern Calif., 1966, p. 1-29.
25) P. Poulsen and D. R. Miller, "The Energy Balance and Free-Jet Expansions of Polyatomics", in Rarefied Gas Dynamics edited by J. L. Potter (Progress in Astronautics and Aeronautics, Vol. 51, 1977), p. 899-911.